

All-dielectric light concentrator to subwavelength volumeS. S. Vergeles,^{1,2} A. K. Sarychev,^{2,3} and G. Tartakovskiy⁴¹*Institute for Theoretical Physics of RAS, Chernogolovka 142432, Russia*²*Moscow Institute of Physics and Technology, Dolgoprudny 141700, Russia*³*Institute of Applied and Theoretical Electrodynamics, Moscow 125412, Russia*⁴*Advanced Systems and Technologies, Inc., Irvine, California 92618, USA*

(Received 24 November 2015; revised manuscript received 12 December 2016; published 2 February 2017)

Concentration of light into a nanospot is essential for the heat assisted magnetic recording, biomedical imaging, sensing, and nanolasers. We propose a novel all-dielectric optical field concentrator, which focuses the light, pumped through the waveguide, into a hot nanospot, which is much smaller than the wavelength. The dissipative loss, which is characteristic to a plasmonic nanoantenna, is absent in the dielectric concentrator. Therefore, the detrimental thermal effects almost vanish, which gives an opportunity to use the concentrator for the heat-assisted magnetic recording. The electric field is much enhanced in the proposed new device at the vertex of the dielectric beak, which is attached to the dielectric resonator. The resonator in turn is pumped through the special waveguide. The electric field enhancement and concentration is achieved by longitudinal polarization of the beak vertex, which is exposed to an electric field generated by the pumped resonator. The spatial scale of the hot spot, where the field concentrates, is determined by the curvature of the vertex and can be of few nanometers. We take as a design concept the cylindrical waveguide, the spherical resonator, and the elliptic beak. The rectangular, 2.5-dimensional design of the light concentrator is also considered.

DOI: [10.1103/PhysRevB.95.085401](https://doi.org/10.1103/PhysRevB.95.085401)**I. INTRODUCTION**

The main achievement of the modern plasmonics is the concentration of light into nanospots that are much smaller than the wavelength. Nanospot concentration is beneficial for various applications: biomedical imaging and sensing, optical microscopy with single-molecule resolution [1], heat assisted magnetic recording (HAMR) [2,3], QED studies [4], nanolasers, etc. Until now, plasmonic metal nanoantennas, subwavelength apertures [5], or metallic near field concentrators (NFCs) are used for this purpose. Optical field enhancement and concentration is achieved in NFC by excitation of the surface plasmons [6,7]. The main advantage of the metal NFC is their capabilities to localize plasmonic modes, which can be excited by the incident transverse em wave. However, the metal NFCs have large optical loss so we propose a novel all-dielectric NFC, which allows us to focus the light into a subwavelength hot nanospot, without the dissipative loss. The detrimental thermal effects almost vanish in the dielectric NFC opening new opportunities in magnetic recording [8–10] and optical pumping.

Optical microcavities can greatly enhance light-matter interactions by storing optical energy in small volumes. The ability to concentrate light is important not only to fundamental physics studies, but also to practical device applications. Optical microcavities confine light to small volumes by resonant recirculation. Devices based on the optical microcavities are already indispensable for a wide range of applications and studies. For example, microcavities made of active III-V semiconductor materials control laser emission spectra to enable long-distance transmission of data over optical fibers; they also ensure narrow spot-size laser read/write beams in CD and DVD players. In quantum optical devices, microcavities can force the atoms or quantum dots to emit spontaneous photons in a desired direction or can provide an environment where dissipative mechanisms such as spontaneous emission

are overcome so that quantum entanglement of radiation and matter is possible (see, e.g., [4,11,12]).

Electromagnetic resonances can be excited in any piece of a low-loss dielectric. Yet, the quality factor Q is very different for various em modes so that some of them are very lossy even in the rather large resonator [13]. Among all em modes the whispering-gallery modes (WGMs) have high Q . Consider a light beam propagating in a circular disk or a sphere via consecutive reflections from the boundary. The rotational symmetry of the cavity shape keeps the angle of incidence constant, and the condition for total internal reflection is maintained. The phase delay for light traveling one circle along the boundary must be equal to $2\pi m$ ($m = 1, 2, 3, \dots$), so that the returning field has the same phase as the original field and a steady state is reached [14]. High quality WGM resonators are used for many applications including microlasers and sensors [15,16]. Yet, high precision is required in positioning the coupler with respect to the cavity boundary in order to obtain sufficient output while avoiding a dramatic reduction of the quality factor (Q spoiling). An alternative way to increase output to the free space is modifying the resonator boundary. After realization of the semiconductor microdisk lasers, Levi *et al.* [17] achieved directional output by introducing a tab on the disk circumference. The same shape and the inverted version (a notch) had been used [18] for the same purpose and for mode discrimination. A linear decrease of the radius of a circle with the polar angle gives the spiral shape with a localized stepped defect [19,20], which demonstrates much enhancement of local em field at the setback as well as unidirectional light emission. Our NFC is similar in a sense to these WGM notched resonators since the NFC consists of the dielectric resonator with attached nanobeak, where the near field concentrates.

The electric and magnetic fields concentration in the dielectric microstructures attracted a lot of attention in recent years [15,21]. The electric field enhancement in-between

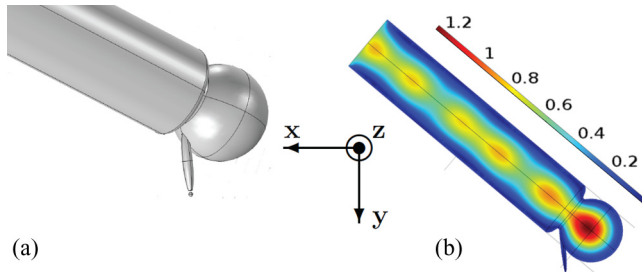


FIG. 1. (a) NFC consisting of a cylindrical silicon waveguide with radius ρ , spherical resonator of radius a , and prolate elliptical nanobeam. (b) Numerical simulation of the magnetic field $|H|$ (A/m), which is pumped in the resonator through the waveguide ($\rho = 107$, $a = 110$ nm, $\lambda = 900$ nm). Magnetic dipole resonance is excited along z axis, i.e., perpendicular to the page; the reflection at the junction between the waveguide and the resonator is rather small so the field is almost not modulated in the waveguide.

two neighboring resonating dielectric spheres was predicted [22] and observed in the experiment [23] for the nanodimer consisting of the silicon nanocylinders of diameter 140 nm, height 150 nm, and gap 30 nm. The chain of six dielectric nanoparticles was suggested as Yagi-Uda antenna [24]. The dielectric Yagi-Uda antenna greatly increases the radiation of a dipole placed between first and second particles. It is clear that the antenna will concentrate the incident light in the same point. Enhanced light focusing was proposed and observed in the work [25], where the authors investigate a ring of plasmonic metal nanoparticles interacting with each other but also with an adjoining dielectric microresonator. The plasmon resonance in the plasmonic ring results in the greater increase of the em field near the surface of the dielectric microresonator far away from the ring. Note that the electric field is much less enhanced in the case of the spatially separated metal clusters and dielectric microresonators [26]. The light propagation in the dielectric metamaterials is discussed in the review [27]. For example, the em wave can be very confined in a subwavelength scale in the dielectric waveguide with anisotropic cladding [28]. The electric field concentration due to a resonance between periodic dielectric rectangular resonators was simulated [29], and super resolution of the resonate microstructures can be achieved by a dielectric microsphere (see [30] and references therein). The enhancement of the optical nonlinearity was observed [31] due to the magnetic resonance in the system of four closely packed dielectric disks. The effective absorption of em energy in the periodic semiconductor metafilms was investigated for the solar cells (see [32] and references therein). The strong electric field enhancement and SERS in the periodic metafilms, constructed from the dielectric microbeams, was obtained in [33,34] for microwave and optical spectral ranges. The distributed dielectric resonances in the randomly faceted ceria metafilms were also considered [35–37]. The dielectric metamaterials can be used for the effective biosensing [38]. Preliminary description of the NFC was published in [39].

In the proposed device the electric field is very enhanced at the vertex of the dielectric beam, which is attached to the dielectric resonator (Fig. 1). The field enhancement at the apex of the sharp dielectric beam can be understood as follows [40]: the external driving field, polarized along the

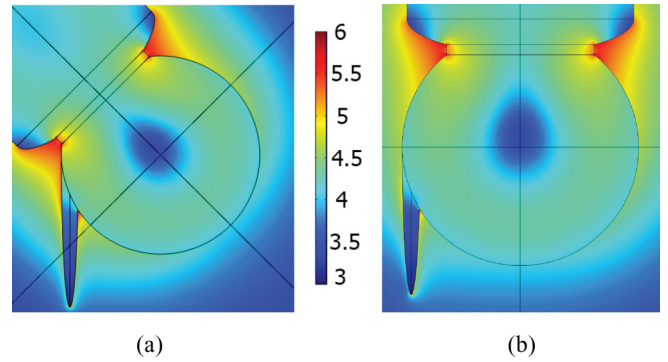


FIG. 2. (a) Electric field $\ln|E|$ (V/m) excites beam: (a) inclined waveguide orientation, beam length $b = 150$ nm; (b) vertical waveguide orientation, $b = 130$ nm; small axis of elliptical beam $g = 11$ nm, spherical resonator has radius $a = 110$ nm, and radius of the waveguide $\rho = 107$ nm.

beak axis, drives the bounded electrons periodically forth and back along the beak shaft with the same frequency as the exciting field. Because of the small surface area near the apex the uniform displacement of the bounded electrons gives rise to a huge surface charge accumulation at the apex. These charges generate a secondary field which is seen in Fig. 2 as enhanced field. The enhancement of the longitudinal electric field at the vertex can be achieved for any optically dense material, including a transparent dielectric (see, e.g., [15,41]). The problem is how to convert the incident light into a longitudinal electric field. A simple waveguide does not produce a considerably localized longitudinal electric field [42], which is necessary to excite the beam. In recently proposed metal NFC [43], the specially designed plasmonic lenses produce the longitudinal electric field. In contrast to the previous works, we propose to excite the dielectric beam through the waveguide ended by the optic resonator, which accumulates em energy. The waveguide is matched with the resonator. The em energy, pumped through the waveguide, accumulates in the resonator and effectively excites the beam, attached to the resonator. Note the WGMs were efficiently channeled into an attached waveguide without additional loss [44]. A robust and generic mechanism was suggested to achieve there unidirectional output from wave-chaotic microcavities.

II. TRANSFORMATION FROM TRANSVERSE TO LONGITUDINAL FIELD

We propose to outfit the end of the waveguide with the spherical Mie resonator. When the resonator is tuned to match the waveguide modes, it strongly influences the spacial structure of em field. The strongly localized longitudinal electric field is produced. Thus, NFC takes the form of the pumped resonator, where the electric field concentrates at the vertex of the attached beam [Fig. 1(a)]. The field is maximized at the vertex. We will use semiquantitative analysis of the NFC elements, namely the spherical resonator, the beam, and the cylinder waveguide feeding. We also present computer simulations of the silicon NFC operating in the red and near-infrared spectral range ($\lambda > 800$ nm), where the silicon

permittivity $\varepsilon \simeq 15$ (see [45,46]); the ohmic loss is neglected being much smaller than the radiation loss. The permittivity of the surrounding space is equal to 1 and the harmonic time dependence $\sim \exp(-i\omega t)$ is assumed for all the em fields and currents.

For the fixed frequency range the quality factor Q of a dielectric resonator increases with increasing its size. It is possible to find a larger number of long-lived modes and the decay time increases. We are interested in the high Q modes that are not fully confined but have a sufficient large external component. Such modes are dumped by the beak attached to the resonator as it is discussed in Sec. V and Appendix B. Hence, we use the simplest spherical resonator, where the magnetic dipole resonance is excited. The magnetic dipole mode has a sufficient high quality factor Q , small volume, and electric field spilled out of the resonator. The em radiation is minimalized in consequence of the solenoid structure of the electric field in the mode. Good enough parameters have electric dipole resonance. Still our computer simulations show that a subwavelength waveguide is better matched with a magnetic dipole mode.

The magnetic dipole Mie resonance is excited in the spherical resonator of radius a in such a way that the average magnetic field is parallel to the “ z ” axis, which is perpendicular to the plane of Figs. 1(b)–6. The electric vector potential \mathbf{A} has only nonzero z -component A_z so that $\mathbf{E} = \text{curl } \mathbf{A}$ and $\mathbf{H} = \text{curl } \mathbf{E}/ik$, where the wave vector $k = \omega/c$ and ω is the resonance frequency. The external electromagnetic field is given by the potential $A_z^e = E_0 u_a^2 \exp[ik(r-a)]/[ku(n-ia_u)]$, where the dimensionless coordinate $u = knr$, $u_a = kna$, the refractive index $n = \sqrt{\varepsilon}$, and \mathbf{r} is the radius-vector. The radiation boundary conditions are imposed at infinity. The internal vector potential is chosen in such a way that at the resonator’s surface $r = a$ the boundary conditions are automatically full field for the electric field and for the normal component of the magnetic field: $A_z^i = -E_0 \sin(u)/[knu f(u_a)]$, where the function f is defined by the following equation:

$$f(u) = \frac{u \cos(u) - \sin(u)}{u^2}. \quad (1)$$

The third boundary condition for the tangential component of the magnetic field gives the dispersion equation for the resonance frequency

$$u_a \cos u_a + (n^2 - 1 - in u_a) \sin u_a = 0. \quad (2)$$

The resonance frequency for the first resonance can be estimated as

$$\omega = \omega_1 - i\omega_2 \approx (\pi c/an)(1 - n^{-2} - i\pi n^{-3}) \quad (3)$$

for the optically dense medium, $n \gg 1$. The imaginary part ω_2 of the resonance frequency gives the radiation loss. Because of the radiation condition $E \sim H \sim \exp(ikr)$, $r \rightarrow \infty$; the solution for the mode has to decay in time. It is therefore a quasibound state with complex-valued frequency ω ; $\text{Im}(\omega) < 0$. Moreover, the fields diverges as $\sim \exp[\text{Im}(k)r]$ with $\text{Im}(k) = \text{Im}(\omega)/c < 0$ as the radial coordinate r tends to infinity. Hence, the quasibound state is strictly speaking not normalizable. The divergence does not affect the angular distribution of the emitted light.

To describe the spatial structure of the em field it is convenient to introduce the spherical coordinates $\{r, \theta, \varphi\}$, where axis z is perpendicular to Fig. 1(b). At the considered magnetic resonance the electric field \mathbf{E} rotates around axis z , i.e., it has the tangential φ component only. Then the internal electric field ($r < a$) can be written as

$$\begin{pmatrix} E_x^i \\ E_y^i \end{pmatrix} = E_0 \sin \theta \frac{f(u)}{f(u_a)} \begin{pmatrix} \sin \varphi \\ -\cos \varphi \end{pmatrix}, \quad (4)$$

where the function f is given by Eq. (1). The outward electric field ($r > a$), which excites the beak, can be written as

$$\begin{pmatrix} E_x^e \\ E_y^e \end{pmatrix} = E_0 \sin \theta \frac{n - iu}{n - iu_a} \left(\frac{a}{r}\right)^2 \exp[ik(r-a)] \begin{pmatrix} \sin \varphi \\ -\cos \varphi \end{pmatrix}, \quad (5)$$

where E_0 is the surface electric field at the equator of the resonator, i.e., $r = a$ and $\theta = \pi/2$. The magnetic field in and out of the resonator is obtained by substitution of Eqs. (4) and (5) in the Maxwell equations. The amplitude of E_0 in Eqs. (4) and (5) is determined by em energy pumped into the resonator. We obtain that the electric field E^e has a “ y ” component, which is parallel to the beak shown in Fig. 1. This longitudinal field effectively excites the beak. The quasibound state (5) approximates the external field for the distance from the resonator $r < 1/\text{Im}(k) \gg a$.

III. POLARIZATION OF A PROLATE BODY PLACED IN NONUNIFORM ELECTROMAGNETIC (EM) FIELD

In the proposed NFC the electric field concentrates in the dielectric beak, which is attached to the spherical resonator. The outward field of the resonator field, given by Eq. (5), excites the beak. We consider now an important nanophotonic problem, namely the field distribution in the vicinity of the much prolated body, which is placed in an inhomogeneous electric field. The em wave scattering by a dielectric ellipsoid is a classical problem of the classical electrodynamics. In recent years significant progress is achieved in the “Mie theory” for scattering by a dielectric ellipsoid (see [47] and references therein). The problem is reduced to the infinite set of the linear equations for the spatial harmonics. The number M of the harmonics, which should be considered to approximate the near field, depends on the inhomogeneity of the local field. The electric field concentrates in the vicinity of the apex of the high-refractive-index, prolate ellipsoid we are interested in. The spatial scale of the region, where the field concentrates, is on the order of the curvature of the apex $R_0 = g^2/b$, where $g \ll b$ are semiaxes of the ellipsoid. Then the number of the spatial harmonics and, correspondingly, the number of the linear equations to be solved estimates as $M \sim b/R_0 = (b/g)^2 \gg 1$. Therefore, it is difficult to use the Mie theory for the analytical calculation of the electric field near the prolate high-refractive-index ellipsoid.

We show below that the field and the charge distribution in the much prolated dielectric beak can be found from the ordinary differential equation, which is merely a usual hypergeometric equation. It is assumed, for the simplicity, that the beak in Fig. 1 is the prolate axisymmetrical body of revolution. The axis of the beak is chosen as y axis,

i.e., the beak is a cylinder, in which radius $r(y)$ depends on the coordinate. The developed formalism holds for any shape-function $r(y)$ as soon as $|dr/dy| \ll 1$. The obtained below Eq. (15) gives the field distribution in any smooth cylinder with variable radius. To get insight into the problem we consider now the simple quasielliptical beak, whose radius changes as

$$r(y) = g \left[1 - \left| \frac{y}{b} \right|^{\frac{2}{\alpha+1}} \right], \quad (6)$$

where $|y| < b$ is the coordinate along the beak axis, the semiaxis $g \ll b$, and the exponent $\alpha > -1$. When $\alpha = 0$ Eq. (6) gives the simple elliptic beak. The exponent α defines bluntness/sharpness of the beak apex, namely the curvature of the apex equal to $R = R_0/(1 + \alpha)$, where $R_0 = g^2/b$ is the curvature of the ellipsoid at the end point $y = b$. Note that the condition $|dr/dy| \ll 1$ is violated in the small vicinity of the central point $|y| < g(\frac{g}{b})^{\frac{2}{\alpha+1}}$ when the index $\alpha > 1$. This region, however, does not have much influence on the internal electric field since the surface charge is mainly distributed at the end of the beak as it is discussed below.

We find the internal electric field in the much elongated beak of length $2b \gg g = \max(r)$ and the beak is assumed to be rather smooth. This form factor is typical for the metal tips used in the contemporary experiments [40]. The beak is excited by an inhomogeneous longitudinal field E_y^e given, for example, by Eq. (5). The material of the beak is characterized by permittivity $\varepsilon = n^2$ or complex conductivity $\sigma \equiv -i\omega(\varepsilon - 1)/4\pi$. The internal electric field in the beak $E^b(y)$ is the sum of the external field and the field induced by the electric charge and the current

$$E_y^b(y) = E_y^e(y) - \frac{d\Phi(y)}{dy} + ikA_y(y), \quad (7)$$

where Φ and A_y are scalar and vector potentials correspondingly; the Lorentz gauge is assumed. The transversal field, induced by the current and charge, is neglected since we assume $|dr/dy| \ll 1$. Then the relation between the electric current J and the field E_y^b at the axis of the beak is given by the Ohm law

$$J(y) = \pi[r(y)^2 F_s(y)]\sigma E_y^b(y), \quad (8)$$

where the beak radius $r(y)$ is given by Eq. (6); the function $F_s(y)$ equals $F_s(y) = 2J_1[nkr(y)]/[nkr(y)]$, where J_1 is the first kind of Bessel function. The renormalization of the radius, given by the function $F_s(nkr)$, appears in Eq. (8) due to the nonuniform beak filling with the current when the skin effect is important, i.e., $|n|kg > 1$.

The electric potential Φ is produced by the charge, which is distributed over the surface of the beak. Let $q(y)$ be the linear density of the charge, then the potential at the axis y is given by the integral

$$\Phi(y) = \int_{-b}^b \frac{e^{ik|y-y'|} q(y') dy'}{\sqrt{(y-y')^2 + r(y')^2}}. \quad (9)$$

The electric potential can be divided into singular and regular parts. The singular part Φ_0 of the potential Φ is extracted

from Eq. (9) by splitting the integral into two parts $\Phi(y) \equiv \Phi_0(y) + \Phi_1(y)$, namely

$$\Phi_0(y) = q(y) \int_{-b}^b \frac{dy'}{\sqrt{(y-y')^2 + r(y')^2}} = \frac{q(y)}{C(y)}, \quad (10)$$

$$\Phi_1(y) = \int_{-b}^b \frac{q(y')e^{ik|y-y'|} - q(y)}{\sqrt{(y-y')^2 + r(y')^2}} dy', \quad (11)$$

where the dimensionless coefficient $C(y)$ is the linear capacitance, which depends on the radius $r(y)$. To solve the integral in Eq. (10) note that the small term $r(y')^2$ in the square root is only important for $|y - y'| < g$. We replace $r(y') \approx r(y) + (dr/dy)(y' - y)$ by $r(y)$, since it is assumed that $|dr/dy| \ll 1$, obtaining

$$\begin{aligned} \Phi_0(y) &\approx q(y) \ln \left[\frac{\sqrt{(b+y)^2 + r(y)^2} + b + y}{\sqrt{(b-y)^2 + r(y)^2} - b + y} \right] \approx \frac{q(y)}{C(y)}, \\ \frac{1}{C(y)} &= \ln \frac{4(b^2 - y^2)}{r^2(y)}, \end{aligned} \quad (12)$$

where we still suppose that $r(y) \leq g \ll b$. Thus the electric potential in the logarithmic approximation is just proportional to the linear charge density. For the beak, which shape is given by Eq. (6), the linear capacitance equals

$$\frac{1}{C(y)} = \frac{1}{C_0} + \ln \left(\frac{1 - y_2^2}{1 - |y_2|^{\frac{2}{\alpha+1}}} \right), \quad (13)$$

where $y_2 = y/b$ and $C_0 = [2 \ln(2b/g)]^{-1}$ is the linear capacitance of a prolate ellipsoid. The second term in Eq. (13) is on the order of one and it achieves the maximum value $\ln(\alpha + 1)$ for $y \rightarrow b$. Therefore, we can neglect this term in comparison with C_0^{-1} for the case of a much elongated beak when $(2b/g)^2 \gg 1 + \alpha$. Then the linear capacitance $C(y)$ is just a constant $C(y) \approx C_0$.

We now estimate the nonsingular part Φ_1 of the electric potential. The integral for potential $\Phi_1(y)$ in Eq. (11) has no singularity at $y = y'$. Therefore the potential $\Phi_1(y)$ gives relatively small correction to the singular potential $\Phi_0(y)$. Yet, the potential Φ_1 can be important since the phase of Φ_1 is shifted with respect to the charge $q(y)$ and, therefore, $\Phi_1(y)$ gives the radiation loss as it is discussed below in Sec. V and Appendix B.

Using the same approach we obtain the vector potential $A_y(y) \approx L(y)J(y)/c$, where $L(y) = C(y)^{-1} = \ln[4(b^2 - y^2)/r^2(y)]$ is the linear inductance, and c is the speed of light. Note the vector potential can be presented in the alternative form $A_y(y) \approx -ikL(y)P_y(y)$, where $P_y(y)$ is the polarization of the beak along its shaft. We substitute the electric potential Φ_0 and vector potential A_y in Eq. (7) and obtain the electric field inside the beak $E_y^b(y)$ in terms of the surface charge $q(y)$ and the electric current $J(y)$ flowing in the beak

$$E_y^b(y) = E_y^e(y) - \frac{d}{dy} \frac{q(y)}{C(y)} + \frac{ik}{c} \frac{J(y)}{C(y)}, \quad (14)$$

where $E_y^e(y)$ is the component of the external field directed alongside the beak. The obtained internal electric field $E_y^b(y)$ we substitute in the Ohm law, use the charge conservation $i\omega q = dJ/dy$, and obtain the equation for the electric current

flowing in the beak

$$J(y) = \pi r(y)^2 F_s(y) \sigma \left[E_y^e(y) - \frac{1}{i\omega} \frac{d}{dy} \left(\frac{1}{C(y)} \frac{dJ(y)}{dy} \right) + \frac{ik}{c C(y)} J(y) \right], \quad J(\pm b) = 0. \quad (15)$$

The internal field at the beak axis equals $E_y^b = J/(\pi r^2 F_s \sigma)$ as it follows from Eq. (8). Note that in the case of strong skin effect ($\text{Re } \sigma \rightarrow \infty$) the internal electric field E_y^b vanishes and, therefore, the expression in the square brackets on the right-hand side of Eq. (15) vanishes also. Then we obtain the well known antenna ‘‘microwave’’ equation [48,49] for the current in the thin metal wire antenna.

There is an important particular case of the prolate beak given by Eq. (6), where the semiaxes ratio is large enough $(b/g)^2 \gg \alpha$. Hence the capacitance and inductance, given by Eq. (12), do not depend on the position $C = 1/L \approx 1/[2 \ln(2b/g)]$. We consider a rather small beak $b \ll \lambda$ and neglect, for simplicity, the skin effect and inductance. Then Eq. (15), which can be rewritten in terms of the internal field $E_y^b = J/(\pi r^2 \sigma)$, takes the form of the hypergeometric equation

$$(y_1 - 1)y_1 \frac{d^2 E_y^b(y_1)}{dy_1^2} + 2(2y_1 - 1) \frac{dE_y^b(y_1)}{dy_1} + (2 + D_0)E_y^b(y_1) = D_0 E_y^e(y_1), \quad (16)$$

for the beak field E_y^b , where the dimensionless coordinate $y_1 = (1 - y/b)/2$, and the parameter

$$D_0 = 2/[n_y(\varepsilon - 1)], \quad (17)$$

where the depolarization coefficient $n_y = (g/b)^2 \ln(2b/g)$. Equation (16) has a simple analytical solution considered in detail in Appendix A. Surprisingly, the deviation of field E_y^b from the external field E_y^e inside the beak is determined by the only parameter D_0 , where the depolarization coefficient n_y is supposed to be small $n_y \ll 1$. In the case of a strongly elongated beak, $D_0 \gg 1$, the internal field is close to the applied field $E_y^b \simeq E_y^e$, see Eqs. (A3) and (A4). On the contrary, when the parameter $D_0 \leq 1$ and the dielectric permittivity ε is large, one can alternate the electric field inside the beak by means of the beak geometry variation.

IV. FIELD ENHANCEMENT AT THE APEX OF THE DIELECTRIC BEAK

In the proposed NFC the beak has the form of the prolate ellipsoid and it is placed in the equatorial plane x, y ($\theta = \pi/2$) with the shaft parallel to the y axis as it is shown in Fig. 1. The center of the beak is located on axis x at the distance d from the center of the resonator. The internal field $\{E_x^b, E_y^b\}$ is estimated as the field in the prolate ellipsoid placed in the external field $\{E_x^e, E_y^e\}$ given by Eq. (5). We use Eq. (A4) to calculate the electric field component parallel to the beak axis $E_y^b(y)$ inside the beak. The field, which is perpendicular to the beak shaft, is approximated as $E_x^b = E_x^e/[1 + n_x(\varepsilon - 1)]$, where the transversal depolarization factor $n_x \cong 1/2$ for $g \ll b$. The field intensity I_s on the outer surface of the beak $I_s(y) = \varepsilon^2 |\mathbf{E}^b \cdot \mathbf{n}^b|^2 + |\mathbf{E}^b - (\mathbf{E}^b \cdot \mathbf{n}^b)\mathbf{n}^b|^2$, where \mathbf{n}^b is the unit

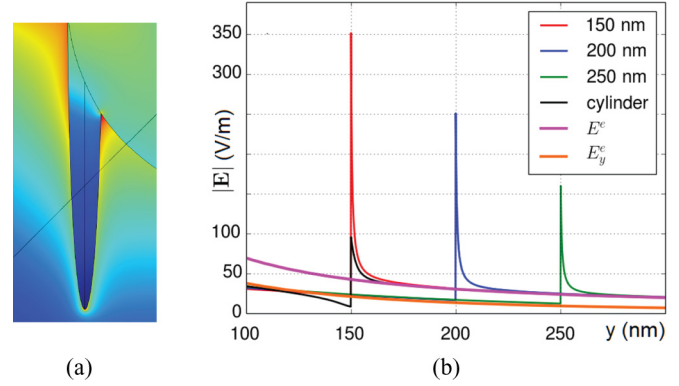


FIG. 3. (a) Dielectric elliptical beak guides electric field: length $b = 150$ nm, small axis $g = 11$ nm, and resonator radius and wavelength are $a = 110$ nm and $\lambda = 900$ nm, correspondingly. The units are the same as in Fig. 1. (b) $|E^b(y)|$ -field profile along the shaft of the beak of various length b , the apex curvature $R_0 = 1$ nm; external E^e field and its tangent projection E_y^e in the absence of the beak are also shown; the internal field $|E_y^b|$ equals the applied field $|E_y^e|$ for elliptical beak, whereas $|E_y^b| \ll |E_y^e|$ near the end of the cylindrical beak; note the electrical field concentrates in the nanovolume indeed.

vector normal to the surface. The field enhancement at the beak surface is shown in Fig. 3. The field intensity at the vertex of the beak is estimated from Eqs. (5) and (A4) as

$$I_s(b) \simeq |E_0|^2 (\varepsilon d a^2)^2 \frac{1 + (b^2 + d^2)k^2}{(b^2 + d^2)^3 (1 + a^2 k^2)}, \quad (18)$$

where d is the position of the beak, E_0 [Eq. (5)] is the field at the surface of the resonator, and $k \simeq \pi/(na)$ [see Eq. (2)] is the resonant wave vector. For $n \gg \pi$ the beak intensity $I_s(b)$ achieves maximum value $I_m \simeq |E_0|^2 \varepsilon^2 (a/b)^4$ for $d \simeq a$. The maximum intensity estimates as $I_m \approx 13|E_0|^2$ for the silicon resonator with the resonant wavelength $\lambda_r = 900$ nm, $\varepsilon \cong 15$, and geometric sizes $a = 110$ nm, $b = 150$ nm, $g = 11$ nm (see Fig. 3). The cascade enhancement of the electric field is achieved: first of all, there is a resonance in the dielectric resonator, second, the resonant field is further amplified due to the longitudinal polarization of the beak.

The electric field at the closest vicinity of the vertex is approximated as the field outside the dielectric ellipsoid (see, e.g., [50] Sec. 8). We use this known solution for the outward field in the vicinity of the vertex of the much prolated ellipsoid. The field intensity along the beak shaft changes as

$$I(y_b) = I_s(b) \left(\frac{2y_b/\varepsilon + 1}{2y_b + 1} \right)^2, \quad (19)$$

where $I_s(b)$ is given by Eq. (18), $y_b = (y - b)/R_0 > 0$ is the dimensionless distance from the vertex, and $R_0 = g^2/b$ is the curvature of the elliptical beak at its vertex. Note the outward beak normal \mathbf{n}^b changes its direction on the elliptical curvature scale R_0 . Therefore, the electric field concentrates in the subwave volume $\sim R_0^3 \ll g^3 \ll \lambda^3$ (Fig. 3). The localization scale and the intensity of the local field are on the same order of magnitude as in the plasmonic nanoantennas [51]. The size of the hot spot at the beak vertex further shrinks when the apex becomes more sharp, that is the parameter α in Eq. (6) increases above zero and the apex curvature $R = R_0/(1 + \alpha)$ decreases.

We speculate that the above estimates for the field holds for the quasielliptical beak, which shape is given by Eq. (6), when it is elongated enough so that $2\ln(2b/g) \gg \ln(1 + \alpha)$ and the linear capacitance of the beak is still a constant [see discussion at Eq. (13)]. In the opposite case of the straight cylinder, which corresponds to the parameter $\alpha \rightarrow -1$ in Eq. (6), the field $|E_y^b| > |E_y^e|$ just outside of the end of the cylindrical tip. However, it is much less enhanced in comparison with a prolate ellipsoid, as it is shown by the black curve in Fig. 3(b), since the surface charges, distributed at the base of the cylinder beak, screen the external field.

V. EXCITATION OF RESONATOR AND BEAK

The spherical silicon resonator with attached beak is pumped through the dielectric waveguide. Therefore in contrast to ANSOM we can directly deliver the electric power to the vertex of the beak without widespread exposure. We consider the silicon cylindrical waveguide attached to the resonator as it is shown in Figs. 1 and 2. Two configurations of the beak and the waveguide were considered in the computer simulations. The beak was attached near the the connection of the waveguide with the resonator or the beak was opposite to the waveguide, as it is shown in Figs. 2(a) and 2(b), correspondingly. It is interesting to note that em field is more enhanced in the inclined beak. We speculate that the additional enhancement is due to the em field which is concentrated in the interface between waveguide and the resonator [see also the discussion below Eq. (20)].

To effectively pump the resonator, the backward reflection of the light into the waveguide should be minimized. The reflectance R_w at the interface between the waveguide and the resonator can be estimated as $R_w \cong |Z_w - Z_r|^2 / |Z_w + Z_r|^2$, where Z_r and Z_w are the impedances of the resonator and waveguide, respectively. The problem of the effective pumping of the dielectric resonator is similar to the problem of an effective excitation of the resonance dielectric antenna (RDA). RDA is an important line in research and design of the compact antennas for the mobile devices including GPS [52,53]. The appertura coupled spherical and semispherical RDAe were theoretically and experimentally studied [54–57]. When the frequency of the external field is close to the resonance of the dielectric resonator the single mode approximation can be used to estimate the input impedance. Then the dielectric resonator input impedance Z_r is given by the equation $[\mathbf{n}^r \times [\mathbf{n}^r \times \mathbf{E}_0]] = Z_r[\mathbf{n}^r \times \mathbf{H}_0]$, where \mathbf{E}_0 and \mathbf{H}_0 are the fields at the surface of the resonator given by Eq. (5) and \mathbf{n}^r is the surface normal. The structure of the em field in the magnetic resonator results in the impedance $Z_r = -iu_a f(u_a) / \{n[f(u_a) + \sin(u_a)]\}$, which remains the same at any point of the interface of the resonator, here the function f is given by Eq. (1) and resonance value u_a is given by the solution of Eq. (2). For the wavelength $\lambda_r = 900$ nm the impedance equals $Z_r \approx 0.454 - 1.108i$ for the silicon resonator. The real part of the impedance Z_r is always positive, which follows from the energy conservation law. The imaginary part of Z_r is negative and it is much larger than $\text{Re}(Z_r)$. It is not surprising that the impedance is almost inductive for the magnetic resonance. To be effectively

pumped the resonator impedance Z_r should be matched to the impedance Z_w of the cylinder waveguide.

There is enormous literature devoted to the cylindrical and other dielectric optic waveguides since the problem is central for the modern telecoms. It is well known that the cylindrical waveguide, whose radius is much less than the wavelength, always support so-called dipole mode. In the dipole mode the electrical and magnetic fields are almost uniform in the waveguide. Outside the waveguide they have angular dependence similar to the $2d$ dipole field. When the radius ρ of the dielectric waveguide is sufficiently large $\rho kn > 1$, the electromagnetic wave is well confined inside. Then the waveguide impedance, calculated as above from the equation $[\mathbf{n}^r \times [\mathbf{n}^r \times \mathbf{E}^w]] = Z_w[\mathbf{n}^r \times \mathbf{H}^w]$, yields the value of $Z_w = n^{-1} \approx 0.252 \ll |Z_r|$, that is the interface reflectance $R_w \cong 0.65$. Note that the vector \mathbf{n}^r has the same direction in both equations for the impedances Z_r and Z_w since the axis of the waveguide is assumed to be normal to the resonator interface.

The dipole mode is preserved in the waveguide even when its radius ρ vanishes. Yet, the spatial distribution of the em field qualitatively changes when the radius ρ decreases up to zero. We obtain the em field by standard matching the linear combination of TE and TM dipole modes inside and outside a dielectric waveguide. Thus an obtained dispersion equation for the phase constant q results in the following result. When the waveguide radius ρ decreases below the critical value $\rho_c = v_{01} / (k\sqrt{n^2 - 1})$, where v_{01} is the first zero of the first-kind, zero-order Bessel function J_0 , the phase constant estimates as

$$q = k\sqrt{1 + \frac{4}{(\rho k)^2} \exp\left[-\frac{(n^2 + 1)J_0(p)}{p J_1(p)} - 2\gamma\right]}, \quad (20)$$

where γ is the Euler constant, parameter $p = \rho k\sqrt{n^2 - 1}$, and J_0 and J_1 are the Bessel functions of zeroth and first orders, correspondingly. That is the phase constant q is exponentially close to the wave vector k and, therefore, electromagnetic field spills out of the waveguide. The outside electromagnetic field takes the shape of the dipole wave and spreads all over the space. In this case, the waveguide impedance Z_w depends on the coordinates and takes almost any value in the plane perpendicular to the waveguide axis. The waveguide radius used in our simulations is 100 nm $\approx 1.2\rho_c$, which corresponds to the compromise between minimization of the waveguide radius and the waveguide mode localization.

The junction between the resonator and the waveguide is optimized by introducing a tapered waveguide “waist,” whose radius is less than the critical radius ρ_c . We use the waveguide waist with radius 65 nm and length 9 nm to match the waveguide with the resonator and reduce the reflectance $R_w < 0.1$ so that the wave, shown in Fig. 1(b), is almost nonmodulated in the waveguide. Therefore, almost all external power is pumped into the resonator, where the electric field intensity of $|E_0|^2$ is increased Q times with respect to the pumping field. The resulting intensity enhancement G at the beak vertex could be as large as $G \sim Q\varepsilon^2(a/b)^4 \gg 1$.

When considering the matching between the waveguide and the resonator we do not take into account the beak, which is attached to the resonator. Consider now the impact of the beak

on the em field oscillations in the dielectric resonator. The electric energy, accumulated inside the resonator, estimates as $\mathcal{H}_r = \varepsilon \int_{\text{in}} |E^{\text{in}}(\mathbf{r})|^2 dV$, substituting here the internal field from Eq. (4) and resonance value $u_a \approx \pi$ from Eq. (3) we obtain $\mathcal{H}_r \simeq \frac{1}{6} a^3 \varepsilon |E_0|^2$, where E_0 is the electric field at the equator of the resonator [see Eq. (4)]. We have shown above [see discussion at Eq. (17)] the internal field in the much prolated beak is close to the external field, which excites the beak. Then the beak electric energy estimates from Eq. (5) as $\mathcal{H}_b \sim \varepsilon V_b |E_0|^2$, where $V_b \sim g^2 b$ is the beak volume. The relative shift of the resonance frequency due to the beak is about $\Delta\omega/\omega \sim \mathcal{H}_b/\mathcal{H}_r \sim g^2 b/a^3$. We consider the beak, whose length is about the resonator radius a , then the resonance frequency shift due to the beak estimates as $\Delta\omega \sim \omega_1 (g/a)^2$. This shift of the resonance frequency should be compared with the radiation width of the resonance $\omega_2 \sim \omega_1 \pi n^{-3}$ [see Eq. (3)]. When the refractive index $n \leq (a/g)^{2/3}$ the resonance frequency shift is on the order of the radiation width and, therefore, can be neglected for a qualitative analysis.

The radiation width itself increases since the beak functions as an antenna that radiates em energy accumulated in the resonator. The radiation loss in the resonator without the beak estimates as $Q^r \sim \mathcal{H}_r \omega_2 \sim \omega_1 a^3 n^{-1} |E_0|^2$, where the resonance frequency ω_1 and relaxation frequency ω_2 are given by Eq. (3). The beak radiation Q^b is investigated in the details in Appendix B. Yet, it can be roughly estimated as dipole radiation $Q^b \sim (g^2 b)^2 |j|^2 k^3 \omega_1^{-1}$, where j is the density of the displacement current in the beak. In the much prolated beak, when the parameter $D_0 \gg 1$ [see Eqs. (17) and (A3)], the inside field is close to the external field. Then the displacement current approximates as $|j|^2 \sim (\varepsilon \omega_1)^2 |E_0|^2$ and the radiation loss $Q^b \sim \omega_1 n (g^2 b)^2 a^{-3} |E_0|^2$, where we take into account that the resonance wave vector $k \sim (an)^{-1}$. In the considered NFC the beak length $b \sim a$, hence, $Q^b \sim \omega_1 n g^4 a^{-1} |E_0|^2$. Since the beak loss Q^b is less than the resonator loss Q^r , that is the ratio $Q^b/Q^r \sim \varepsilon (g/a)^4 \ll 1$, we can neglect for the qualitative consideration the influence of the beak radiation on the considered magnetic resonance.

We performed our computer simulations in FEMLAB environment. The whole system, including the beak, the resonator, and the waveguide, has been surrounded by the perfectly matching layer (PML), with the radius greater than

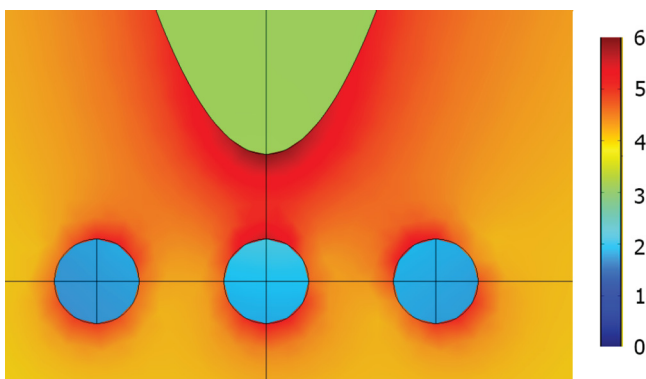


FIG. 4. Tip heats 2 nm magnetic nanoparticles made of alloy FePt [58]; heat production inside the central magnetic particle is 1.4 times greater than in its neighbors.

the vacuum wavelength. The waveguide's port, which is placed near the intersection of the dielectric waveguide and the PML sphere, is used to launch the em wave into the waveguide, which in turn pumps the spherical resonator. In order to demonstrate the capability of light concentration, we simulate the field distribution around three test spherical FePt nanoparticles 2 nm in diameter, placed in the vertex area of the beak, see Fig. 4. Such FePt nanoparticles are often used for a magnetic recording [5,58].

VI. PLANAR, QUASI-TWO-DIMENSIONAL DESIGN FOR THE NEAR FIELD CONCENTRATOR: NUMERICAL SIMULATION OF 2.5-DIMENSIONAL HEATING HEAD ABOVE WAFER WITH Fe-Pt GRAINS

Suppose that we would like to integrate the proposed near field concentrator in the solid state electronics. Then it is convenient to use the layer by layer growth for the fabrication of the waveguide, the resonator, and the tip. The thin film technology is typical for the fabrication nanoscale objects. To reduce the number of the technological steps and simplify the production process the structure should have a right cylindrical

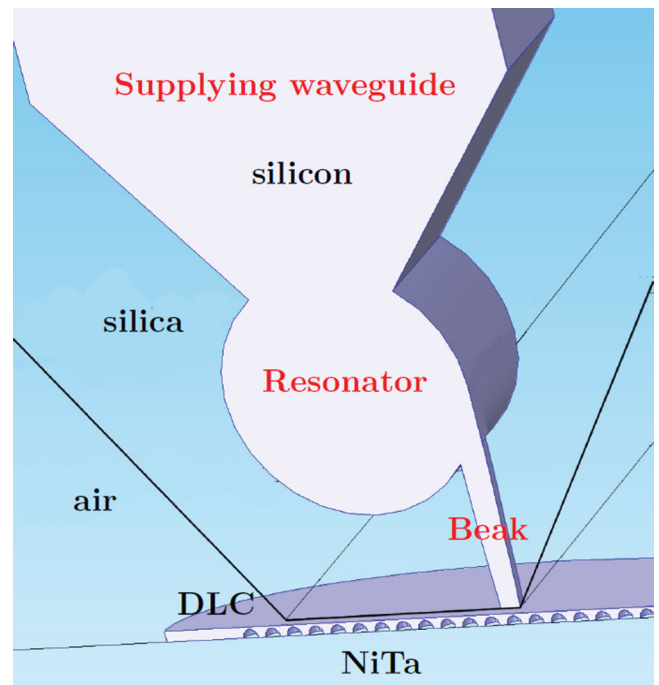


FIG. 5. Rectangular supplying waveguide, disk resonator, and beak of the near field concentrator are made of silicon. The front plane is the cutting plane of mirror symmetry. The lateral faces of the silica cladding are shown by bold black lines, two faces of the cladding parallel to the diamondlike carbon (DLC) substrate are marked by light black lines. DLC layer with equally spaced FePt grains is placed above NiTa substrate. FePt grains of size 14 nm are arranged in the square lattice with period 20 nm. Height of the tip (size in the direction perpendicular to the figure plane) is 16 nm. Disk radius is 110 nm, its height is 210 nm. The gap between the cladding and DLC plate is equal to 5 nm. Optical properties of Fe-Pt alloy were taken from [58], and for silicon from [46]. Permittivity of NiTa alloy we estimate as the arithmetic mean of Ni and Ta permittivities. Permittivity of DLC is estimated as $\varepsilon_{\text{DLC}} = 3.5$ from [59,60].

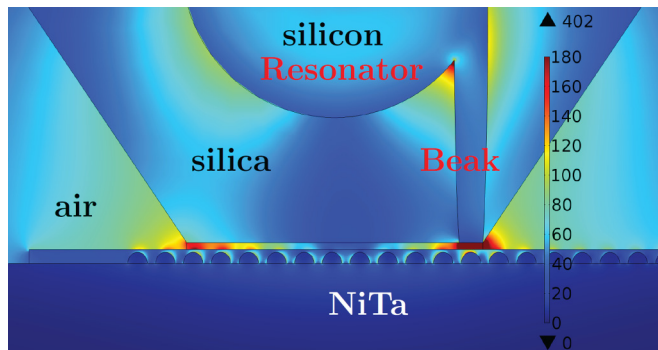


FIG. 6. Electric field distribution below the heating head.

form in the direction of the technological growth, i.e., in the direction perpendicular to the plane of Fig. 5 (z direction). That is the resonator is not spherical but it has a disk shape, the waveguide has rectangular shape, and the beak is an rectangular edge as it is shown in Fig. 5. Note that height of the beak (size in z direction) is less than the height of the disk resonator and the waveguide. The strong em field confined between two rectangular dielectric waveguides was considered in [61–63]. Various disk resonators were investigated for microwaves many years ago [52]. For the optical spectral range anapole resonance as well as magnetodipole resonance in the silicon disk were investigated recently in the computer and real experiments [64,65].

We performed the numerical simulation of em field distribution in 2.5-dimensional (2.5D) silicon NFC as it is shown in Fig. 6. The disk resonator, rectangular beak, and the plane waveguide are embedded in the silica cladding. The disk resonator and the plane waveguide have the same height. The beak has rectangular cross section. Thus constructed 2.5D NFC including the silica cladding can be of a macroscopic size and can be integrated in the modern devices. Thus the NFC can be used for HAMR or local biosensing. To demonstrate HAMR capability of the proposed 2.5D NFC we added substrate, whose structure resembles those considered in [66,67]. The substrate is the diamondlike carbon (DLC) matrix, where Fe-Pt nanograins are distributed. Electric field is much enhanced at the tip of the silicon beak embedded in the silica cladding. We perform the computer simulation of the heating Fe-Pt conducting grains due to the ohmic loss. The heat production rate $\sim \text{Im}(\epsilon_{\text{FePt}})|E|^2$ inside the grains below NFC is shown in Fig. 7. The heat production rate inside the grain just below the

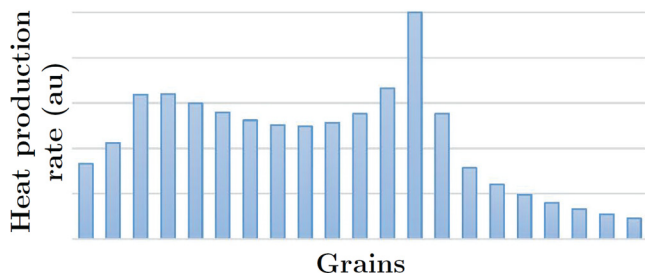


FIG. 7. Heat production rate inside the grains in the central line. The peak corresponds to the grain below the tip as it is shown in Fig. 6.

tip is no less than 1.6 times greater than inside the neighboring grains. Therefore the proposed 2.5D NFC can be successfully used for the local heating with the spatial resolution ~ 10 nm. We speculate that the further optimization would improve the resolution up to ~ 1 nm. Note that the magnesium oxide (MgO), which is also widely used as the substrate for the magnetic recording, has the optical constants close to DLC. Thus, the obtained results are expected to hold for the MgO substrates.

VII. CONCLUSIONS

We propose to use the resonances in specially designed hierarchical dielectric structures to obtain the strong field enhancement at a nanospot. The huge field concentration is achieved without energy loss which is characteristic for the metal particles. Thus the proposed em field concentrator consists of the dielectric resonator and the beak with the sharp apex. The resonator accumulates em energy delivered to the resonator through the waveguide. We find the way to effectively match the resonator and the waveguide. Hence we find how to effectively pump the resonator. The electromagnetic field of the resonator illuminates the beak and creates large electric field at the apex. We speculate it is the generic structure for the dielectric NFCs, which can have a rather peculiar form with many apices. An array of the dielectric NFCs can be used, for example, as SERS substrate, where the luminescent background is damped.

For practical applications the two-dimensional design of the NFS could be preferable. Our computer simulations show that the dielectric edge, protruding from a disk resonator, can also concentrate the em field. The proposed system can be used for the heat assisted magnetic recording, nanosensing, local TERS, and many other applications. Power released in the hot spot can be increased if the proper plasmonic grain [68] is placed near the proposed NFC.

ACKNOWLEDGMENTS

We acknowledge stimulating discussions with A. Bogdanov, S. Burgos, and E. Yablonovitch. This work was partially supported by the program “Fundamental and applied problems of photonics and physics of new optical materials” of Russian Academy of Science. Part of the computer simulations was performed in the Supercomputing Center of the Novosibirsk State University. The numerical simulations were supported by Russian Federation President Grant MK-7373.2015.2.

APPENDIX A: INTERNAL FIELD IN AN ELONGATED QUASISPHEROIDAL BODY PLACED IN AN INHOMOGENEOUS EXTERNAL ELECTRIC FIELD

We consider electric field in the prolate beak, for which the semi-axes ratio is large enough $(b/g)^2 \gg \alpha$. Then Eq. (15) takes the form of the hypergeometric equation (16). The electric field inside the beak is given by the solution of Eq. (16), which is regular for $0 \leq y_1 \leq 1$. For the considered symmetric beak [$r(y) = r(-y)$, see Eq. (6)] the homogeneous Eq. (16) has two independent solutions $F(y_1)$ and $F(1 - y_1)$, where $F(y_1) = {}_2F_1(\frac{3}{2} + iG, \frac{3}{2} - iG, 2, y_1)$ is the standard

hypergeometric function, $G = \sqrt{D_0 - \frac{1}{4}}$. Then the solution of the *inhomogeneous* Eq. (16) has the following form:

$$E_y^b(y_1) = \frac{\pi D_0^2}{\cosh(G\pi)} \left[\int_0^{y_1} t(t-1)W(y_1, t)E_y^e(t)dt - F(y_1) \int_0^1 t(t-1)F(t)E_y^e(1-t)dt \right] \quad (\text{A1})$$

where the dimensionless coordinate $y_1 = (1 - y/b)/2$, the external electric field $E_y^e(y_1)$ is an arbitrary function of y_1 , and the Green function equals $W(y_1, t) = F(y_1)F(1-t) - F(t)F(1-y_1)$. Equation (A1) gives the variation of the internal field in the dielectric beak, which is excited by spatially inhomogeneous external electric field $E_y^e(y_1)$.

Equation (A1) for the internal electric field is much more simplified when the external field expands in the series

$$E_y^b(y_1) = \frac{D_0}{D_0 + 2} \left[E_0 + E_1 \frac{(D_0 + 2)y_1 + 2}{D_0 + 6} + E_2 \frac{(D_0 + 2)y_1[(D_0 + 6)y_1 + 6] + 12}{(D_0 + 6)(D_0 + 12)} + E_3 \frac{(D_0 + 2)y_1\{(D_0 + 6)y_1[(D_0 + 12)y_1 + 12] + 72\} + 144}{(D_0 + 6)(D_0 + 12)(D_0 + 20)} \right], \quad (\text{A3})$$

where the parameter D_0 is given by Eq. (17), $y_1 = (1 - y/b)/2$. This equation replaces the classical equation $E_y^b = E_0 - 4\pi P_y n_y$ for the internal field in the dielectric ellipsoid placed in the *uniform* electric field (see, e.g., [50] Sec. 8). The solution check can be done by the direct substitution of Eq. (A2) or (A3) in Eqs. (16). Recall that the above results are obtained with so-called logarithmic accuracy: it is assumed that not only $(b/g)^2 \gg 1$ but also $2 \ln(b/g) \gg 1$.

Following Eq. (A3), the electric field inside the beak, extrapolated to the vertex $y = b$, i.e., $y_1 = 0$, estimates as

$$E_y^b(b) = \frac{D_0}{D_0 + 2} \left\{ E_0^e + \frac{2}{D_0 + 6} \left[E_1^e + \frac{6}{D_0 + 12} \times \left(E_2^e + \frac{12}{D_0 + 20} E_3^e \right) \right] \right\}, \quad (\text{A4})$$

where D_0 is given by Eq. (17).

APPENDIX B: RADIATION LOSS IN A PROLATE DIELECTRIC ELLIPSOID

The radiation of em waves is a most important loss for a dielectric antenna. For the qualitative analysis, we consider the radiation of a small ($bk < 1$), much prolated dielectric ellipsoid, excited by the uniform external field E_0 . The radiation loss Q^r is expressed in terms of the polarizability as $Q^r = \frac{1}{2}\omega\alpha_2|E_0|^2$, where $\alpha_2 = \text{Im}\alpha$ is the imaginary part of the ellipsoid polarizability α (see, e.g., [50], Sec. 59). The radiation loss is determined by the nonquasistatic part of the electric potential Φ_1 given by Eq. (B1). For a much prolated ellipsoid the singular, quasistatic part of electric potential Φ_0 , given by Eq. (12), is much larger than nonquasistatic potential $\Phi_0 \gg \Phi_1$. Therefore, we can substitute the quasistatic electric charge $q(y) = -dP^b(y)/dy = yE^b(\varepsilon - 1)(g/b)^2/2$

$E_y^e(y_1) = \sum_{m=0}^{\max} E_m y_1^m$. Then the internal field in the beak is also polynomial and equals

$$E_y^b(y_1) = D_0 \sum_{m=0}^{\max} E_m Y_m(y_1), \quad (\text{A2})$$

$$Y_m(y_1) = A_m \sum_{k=0}^m \frac{|\Gamma(k + \frac{3}{2} + iG)|^2}{k!(k+1)!} y_1^k,$$

where the coefficient A_m equals

$$A_m = \frac{m!(m+1)!}{|\Gamma(m + \frac{5}{2} + iG)|^2},$$

and $\Gamma(x)$ is the Euler gamma function.

Suppose, for example, the external field approximates as $E_y^e(y_1) = E_0 + E_1 y_1 + E_2 y_1^2 + E_3 y_1^3$ then the field inside the beak, which shape is given by Eq. (6), equals

in Eq. (11), where $P^b = (\varepsilon - 1)r(y)^2 E^b/4$ is the linear polarization, $E^b \simeq D_0 E_0/(2 + D_0) \simeq E_0/[1 + n_y(\varepsilon - 1)]$ is the field in the ellipsoid [see Eqs. (17) and (A4)], and y is the coordinate along the elliptic axis, i.e., the beak shaft. Then we expand the integrand in Eq. (11) in the power series of k and ignore the constant term obtaining

$$\Phi_1 = -\frac{g^2(\varepsilon - 1)}{2b^2} \left[2y + \frac{1}{6}k^2 y(y^2 - 3b^2) - \frac{2}{9}ib^3 k^3 y \right] E^b, \quad (\text{B1})$$

where b and $g \ll b$ are semiaxes. The vector potential also gives impact in nonquasistatic electric field [see discussion at Eq. (14)]. In the lowest orders of k the vector potential equals

$$A_{y1} = -\frac{1}{c} \int_{-a}^a \frac{J(y_1)e^{ik|y-y_1|} - J(y)}{|y - y_1|} dy_1 \simeq i \frac{g^2 k(\varepsilon - 1)}{4} \left(1 - 3\frac{y^2}{b^2} - i\frac{4}{3}bk \right) E^b, \quad (\text{B2})$$

where $J(y) = -i\omega P^b(y) = -\frac{1}{4}\omega(\varepsilon - 1)g^2[1 - (y/b)^2]E^b$ is the polarization current in the dielectric ellipsoid. Substituting the potentials from Eqs. (B1) and (B2) in Eq. (7) we obtain the corrections to the internal field

$$E_1^b = E^b \frac{g^2}{b^2} (\varepsilon - 1) \left[1 + (kb)^2 \left(\frac{y^2}{b^2} - \frac{1}{2} \right) + i\frac{2}{9}(kb)^3 \right], \quad (\text{B3})$$

due to the nonquasistatic effects. As it was expected, the corrections are small for the much prolated, subwavelength ellipsoid, i.e., $g \ll b$ and $bk < 1$. We neglect the small correction to the internal field, given by first and second

terms in the square brackets in Eq. (B3). However, the third term is very important since it gives the radiation of a small elliptic dielectric antenna. Then Eq. (B3) takes form $E_1^b = i \frac{8}{9} \pi g^2 b k^3 P$, where $P = (\varepsilon - 1) E^b / 4\pi$ is the ellipsoid polarization. On the other hand, we can write for the polarization the following equation: $4\pi P(\varepsilon - 1)^{-1} = E_0 - 4\pi n_y P + i \frac{8}{9} \pi g^2 b k^3 P$, where the second term on the right-hand side is the quasistatic depolarization field. The last equation can be rewritten in terms of the full dipole moment \mathcal{P} of the ellipsoid, namely $\mathcal{P}\alpha_0^{-1} = E_0 + i \frac{2}{3} k^3 \mathcal{P}$, where $\alpha_0 = \frac{1}{3} g^2 b (\varepsilon - 1) [1 + n_y (\varepsilon - 1)]^{-1}$ is the quasistatic polarizability of the dielectric ellipsoid. Thus we obtain the equation for the ellipsoid polarizability, which takes into account the radiation loss

$$\alpha = \frac{\alpha_0}{1 - i \frac{2}{3} \alpha_0 k^3} \quad (\text{B4})$$

and the imaginary part of the polarizability approximates as

$$\alpha_2 \approx \frac{2}{3} \alpha_0^2 k^3 = \frac{2}{27} \frac{(\varepsilon - 1)^2}{[1 + n_y (\varepsilon - 1)]^2} g^4 b^2 k^3, \quad (\text{B5})$$

where $n_y \ll 1$ is the axial depolarization factor of the ellipsoid. In the considered system the silicon permittivity ε is sufficiently large $\varepsilon \gg 1$, the length of the beak is about the resonator radius $b \sim a$, and $n_y \varepsilon < 1$. Then the radiation loss due to the beak polarization estimates as

$$Q^b = \frac{1}{2} \omega_1 \alpha_2 |E_0|^2 \sim \omega_1 g^4 a^{-1} n^4 (ka)^3 |E_0|^2 \sim \omega_1 g^4 a^{-1} n |E_0|^2, \quad (\text{B6})$$

where we take into account that resonance wave vector $k \sim (an)^{-1}$. This equation coincides with the rough estimate in Sec. V.

-
- [1] A. M. Armani, R. P. Kulkarni, S. E. Fraser, R. C. Flagan, and K. J. Vahala, *Science* **317**, 783 (2007).
- [2] W. Challener, C. Peng, A. Itagi, D. Karns, W. Peng, Y. Peng, X. Yang, X. Zhu, N. Gokemeijer, Y. Hsia *et al.*, *Nat. Photon.* **3**, 220 (2009).
- [3] S. Vedantam, H. Lee, J. Tang, J. Conway, M. Staffaroni, and E. Yablonovitch, *Nano Lett.* **9**, 3447 (2009).
- [4] T. Aoki, B. Dayan, E. Wilcut, W. Bowen, A. Parkins, T. Kippenberg, K. Vahala, and H. Kimble, *Nature (London)* **443**, 671 (2006).
- [5] S. Hussain, C. S. Bhatia, H. Yang, and A. J. Danner, *Opt. Lett.* **40**, 3444 (2015).
- [6] J. Schuller, E. Barnard, W. Cai, Y. Jun, J. White, and M. Brongersma, *Nat. Mater.* **9**, 193 (2010).
- [7] L. Novotny and N. van Hulst, *Nat. Photon.* **5**, 83 (2011).
- [8] G. Yuan, E. Rogers, T. Roy, Z. Shen, and N. Zheludev, *Opt. Express* **22**, 6428 (2014).
- [9] J. L. Bohn, D. J. Nesbitt, and A. Gallagher, *J. Opt. Soc. Am. A* **18**, 2998 (2001).
- [10] A. Bouhelier, M. Beversluis, A. Hartschuh, and L. Novotny, *Phys. Rev. Lett.* **90**, 013903 (2003).
- [11] K. J. Vahala, *Nature (London)* **424**, 839 (2003).
- [12] B. Min, E. Ostby, V. Sorger, E. Ulin-Avila, L. Yang, X. Zhang, and K. Vahala, *Nature (London)* **457**, 455 (2009).
- [13] H. Tureci, H. Schwefe, P. Jacquod, and D. Stone, *Prog. Opt.* **47**, 75 (2005).
- [14] L. Rayleigh, *The Theory of Sound* (MacMillan, London, 1896).
- [15] H. Cao and J. Wiersig, *Rev. Mod. Phys.* **87**, 61 (2015).
- [16] M. R. Foreman, J. D. Swaim, and F. Vollmer, *Adv. Opt. Photon.* **7**, 168 (2015).
- [17] A. F. J. Levi, R. E. Slusher, S. L. McCall, J. L. Glass, S. J. Pearton, and R. A. Logan, *Appl. Phys. Lett.* **62**, 561 (1993).
- [18] S. A. Backes, J. R. A. Cleaver, A. P. Heberle, and K. Kohler, *J. Vac. Sci. Technol. B* **16**, 3817 (1998).
- [19] G. D. Chern, H. E. Tureci, A. D. Stone, R. K. Chang, M. Kneissl, and N. M. Johnson, *Appl. Phys. Lett.* **83**, 1710 (2003).
- [20] T. Ben-Messaoud and J. Zyss, *Appl. Phys. Lett.* **86**, 241110 (2005).
- [21] A. I. Kuznetsov, A. E. Miroshnichenko, Y. H. Fu, J. Zhang, and B. Lukyanchuk, *Sci. Rep.* **2**, 492 (2012).
- [22] P. Albella, M. A. Poyli, M. K. Schmidt, S. A. Maier, F. Moreno, J. J. Saenz, and J. Aizpurua, *J. Phys. Chem. C* **117**, 13573 (2013).
- [23] R. M. Bakker, D. Permyakov, Y. F. Yu, D. Markovich, R. Paniagua-Dominguez, L. Gonzaga, A. Samusev, Y. Kivshar, B. Lukyanchuk, and A. I. Kuznetsov, *Nano Lett.* **15**, 2137 (2015).
- [24] A. E. Krasnok, A. E. Miroshnichenko, P. A. Belov, and Y. S. Kivshar, *Opt. Express* **20**, 20599 (2012).
- [25] Y. Hong, M. Pourmand, S. V. Boriskina, and B. M. Reinhard, *Adv. Mater.* **25**, 115 (2013).
- [26] Y. Hong, Y. Qiu, T. Chen, and B. M. Reinhard, *Adv. Funct. Mater.* **24**, 739 (2014).
- [27] S. Jahani and Z. Jacob, *Nat. Nanotechnol.* **11**, 23 (2016).
- [28] S. Jahani and Z. Jacob, *Optica* **1**, 96 (2014).
- [29] J. Zhang, W. Liu, Z. Zhu, X. Yuan, and S. Qin, *Opt. Express* **22**, 30889 (2014).
- [30] A. V. Maslov and V. N. Astratov, *Appl. Phys. Lett.* **108**, 051104 (2016).
- [31] A. S. Shorokhov, E. V. Melik-Gaykazyan, D. A. Smirnova, B. Hopkins, K. E. Chong, D.-Y. Choi, M. R. Shcherbakov, A. E. Miroshnichenko, D. N. Neshev, A. A. Fedyanin *et al.*, *Nano Lett.* **16**, 4857 (2016).
- [32] S. J. Kim, P. Fan, J.-H. Kang, and M. L. Brongersma, *Nat. Commun.* **6**, 7591 (2015).
- [33] A. Ivanov, A. Vaskin, A. Lagarkov, and A. Sarychev, in *Plasmonics: Metallic Nanostructures and Their Optical Properties XII* (SPIE, Bellingham, WA, 2014), Vol. 9163, p. 91633C.
- [34] A. Lagarkov, I. Budashov, V. Chistyayev, A. Ezhov, A. Fedyanin, A. Ivanov, I. Kurochkin, S. Kosolobov, A. Latyshev, D. Nasimov *et al.*, *Opt. Express* **24**, 7133 (2016).
- [35] K. Afanasiev, I. Boginskaya, I. Budashov, A. Ivanov, I. Kurochkin, A. Lagarkov, I. Ryzhikov, and A. Sarychev, in *Metamaterials, Metadevices and Metasystems* (SPIE, Bellingham, WA, 2015), Vol. 9544, p. 95441Y.
- [36] A. Lagarkov, I. Kurochkin, I. Ryzhikov, A. Vaskin, K. Afanasiev, I. Boginskaya, I. Budashov, and A. Sarychev, in *Nanophotonic Materials XI* (SPIE, Bellingham, WA, 2014), Vol. 9161, p. 91610M.
- [37] I. S. Kurochkin, I. A. Ryzhikov, A. K. Sarychev, K. N. Afanasiev, I. A. Budashov, M. S. Sedova, I. A. Boginskaya,

- S. Amitonov, and A. N. Lagarkov, *Adv. Electromagn.* **3**, 57 (2014).
- [38] I. N. Kurochkin, A. K. Sarychev, I. A. Ryzhikov, I. A. Budashov, S. S. Maklakov, S. O. Boyarintsev, and A. N. Lagarkov, *Surface-Enhanced Raman Scattering-Based Biosensors*, Series in Sensors (Taylor and Francis, London, 2014), pp. 97–121.
- [39] S. S. Vergeles and A. K. Sarychev, in *Metadevices and Metasystems*, edited by N. Engheta, M. A. Noginov, and I. N. Zheludev (SPIE, Bellingham, WA, 2015), Vol. 9544, p. 954415.
- [40] L. Cancado, A. Hartschuh, and L. Novotny, *J. Raman Spectrosc.* **40**, 1420 (2009).
- [41] J. M. Gerton, L. A. Wade, G. A. Lessard, Z. Ma, and S. R. Quake, *Phys. Rev. Lett.* **93**, 180801 (2004).
- [42] S. Kato, S. Chonan, and T. Aoki, *Opt. Lett.* **39**, 773 (2014).
- [43] Y. Wang, Z. Du, Y. Park, C. Chen, X. Zhang, and L. Pan, *Opt. Lett.* **40**, 3918 (2015).
- [44] Q. Song, L. Ge, B. Redding, and H. Cao, *Phys. Rev. Lett.* **108**, 243902 (2012).
- [45] M. A. Green, *Solar Energy Mater. Solar Cells* **92**, 1305 (2008).
- [46] J. Bergmann, M. Heusinger, G. Andrä, and F. Falk, *Opt. Express* **20**, A856 (2012).
- [47] B. S. Luk'yanchuk, N. V. Voshchinnikov, R. Paniagua-Dominguez, and A. I. Kuznetsov, *ACS Photon.* **2**, 993 (2015).
- [48] E. Hallen, *Electromagnetic Theory* (Chapman and Hall, London, 1962).
- [49] C. Balanis, *Antenna Theory: Analysis and Design* (John Wiley, New York, 2005).
- [50] L. D. Landau, E. M. Lifshitz, and L. P. Pitaevskii, *Electromagnetics of Continuous Media*, 2nd ed. (Pergamon, Oxford, 1984).
- [51] A. K. Sarychev and V. Shalaev, *Electrodynamics of Metamaterials* (World Scientific, Singapore, 2007).
- [52] R. K. Mongia and P. Bhartia, *Int. J. Microw. Millim.-Wave Comput.-Aided Eng.* **4**, 230 (1994).
- [53] A. Petosa and A. Ittipiboon, *IEEE Antennas Propag. Mag.* **52**, 91 (2010).
- [54] K. W. Leung, K. M. Luk, K. Y. A. Lai, and D. Lin, *IEEE Trans. Antennas Propag.* **41**, 1390 (1993).
- [55] K. W. Leung, *IEEE Trans. Microwave Theory Tech.* **46**, 2117 (1998).
- [56] K. W. Leung and K. W. Ng, *IEEE Trans. Antennas Propag.* **46**, 457 (1998).
- [57] A. A. Kishk, X. Zhang, A. W. Glisson, and D. Kajfez, *IEEE Trans. Antennas Propag.* **51**, 1996 (2003).
- [58] K. Sato, A. Mizusawa, K. Ishida, T. Seki, T. Shima, and K. Takanashi, *Trans. Magn. Soc. Jpn.* **4**, 297 (2004).
- [59] S. Singh, M. Pandey, N. Chand, A. Biswas, D. Bhattacharya, S. Dash, A. Tyagi, R. Dey, S. Kulkarni, and D. Patil, *Bull. Mater. Sci.* **31**, 813 (2008).
- [60] B. Mednikarov, G. Spasov, Tz. Babeva, J. Pirov, M. Sahatchieva, C. Popov, and W. Kulisch, *J. Optoelectron. Adv. Mater.* **7**, 1407 (2005).
- [61] V. R. Almeida, Q. Xu, C. A. Barrios, and M. Lipson, *Opt. Lett.* **29**, 1209 (2004).
- [62] C. Koos, P. Vorreau, T. Vallaitis, P. Dumon, W. Bogaerts, R. Baets, B. Esembeson, I. Biaggio, T. Michinobu, F. Diederich *et al.*, *Nat. Photon.* **3**, 216 (2009).
- [63] Q. Liu, X. Tu, K. W. Kim, J. S. Kee, Y. Shin, K. Han, Y.-J. Yoon, G.-Q. Lo, and M. K. Park, *Sensors Actuators B* **188**, 681 (2013).
- [64] A. E. Miroshnichenko, A. B. Evlyukhin, Y. F. Yu, R. M. Bakker, A. Chipouline, A. I. Kuznetsov, B. Luk'yanchuk, B. N. Chichkov, and Y. S. Kivshar, *Nat. Commun.* **6**, 8069 (2015).
- [65] D. Permyakov, I. Sinev, D. Markovich, P. Ginzburg, A. Samusev, P. Belov, V. Valuckas, A. I. Kuznetsov, B. S. Lukanchuk, A. E. Miroshnichenko *et al.*, *Appl. Phys. Lett.* **106**, 171110 (2015).
- [66] D. Weller, O. Mosendz, G. Parker, S. Pisana, and T. S. Santos, *Phys. Status Solidi A* **210**, 1245 (2013).
- [67] J. Hu, K. M. Cher, B. Varghese, B. Xu, C. Lim, J. Shi, Y. Chen, K. Ye, J. Zhang, C. An *et al.*, *IEEE Trans. Magn.* **52**, 1 (2016).
- [68] P. R. West, S. Ishii, G. V. Naik, N. K. Emani, V. M. Shalaev, and A. Boltasseva, *Laser Photon. Rev.* **4**, 795 (2010).